Integrated multi-band WSS: from design to performance evaluation

(Article begins on next page)

11 February 2024

Integrated multi-band WSS: from design to performance evaluation

Lorenzo Tunesi
Politecnico di Torino, IT
lorenzo.tunesi@polito.it

Ihtesham Khan
Politecnico di Torino, IT
ihtesham.khan@polito.it

Muhammad Umar Masood
Politecnico di Torino, IT
muhammad.masood@polito.it

Enrico Ghillino
Synopsys, Inc., USA
enrico.ghillino@synopsys.com

Andrea Carena
Politecnico di Torino, IT
andrea.carena@polito.it

Vittorio Curri
Politecnico di Torino, IT
curri@polito.it

Paolo Bardella
Politecnico di Torino, IT
paolo.bardella@polito.it

Abstract—Modern day optical communications require ever-increasing bandwidths and capacity, in order to keep up with the growth of traffic and resource-intensive applications. This increase in network capacity can be achieved through the use of the residual capacity of current-day infrastructure, although this requires switching and routing devices capable of wide-band operation in multiple transmission windows. In this work, we describe the design principle, architecture, and performance simulation of a photonic integrated circuit (PIC) based multi-band WSS, which is envisioned to operate on the S+C+L windows. While the architecture is scalable to an arbitrary channel and port count, we showcase a 24-channel implementation deployed on the 400ZR standard, providing both the penalty evaluation through DSP simulations, as well as a footprint evaluation based on the components design.

Index Terms—Multi-band, Photonic Integrated Circuits, Wavelength-Selective Switch, Wide-Band.

I. INTRODUCTION

The optical networking landscape is seeing rapid growth in the required capacity due to emerging technologies and resource-intensive applications, as well as a steady increase in connected devices and traffic.

Service providers can address the issue through two main solutions, namely the deployment of new infrastructures (i.e. fibers), the optimization in management of the current resources, or the implementation of new paradigms exploiting the residual network resources. In this context, new fiber deployment represents the most expensive solution, while optimized management is not generalized and can work only on a case-to-case basis. This leaves the exploitation of the residual network capacity as a promising solution. Modern optical transport standards are based on transparent Wavelength-Division Multiplexing (WDM) over the C-band, allowing a spectral window of up to 4.8 THz [1]. The deployment of techniques such as Band-Division Multiplexing (BDM) would allow the extension of the useful spectral window to encompass the rest of the low-loss propagation window, ranging from the O to the L bands (1260 nm-1625 nm), with a total spectral bandwidth of 50 THz [2].

The deployment of BDM, however, requires ultra-wideband Wavelength-Selective Switches (WSS), which must be able to route and control independently each channel in the transmission spectrum, while limiting frequency-dependant penalties. To this goal, we propose a Photonic Integrated Circuit (PIC) based WSS architecture, which would leverage the benefits of integration, such as low cost, reduced footprint, and high performance, while maintaining the functionalities required for implementation in CDC ROADM nodes.

While the general architecture and structure are described, the simulation results are presented for a 24-channel implementation deployed on the S+C+L bands, considering 100 GHz-spaced 16QAM channels.

II. WSS DESIGN

The proposed WSS architecture represents a PIC-based solution for DWDM multi-band scenarios, scalable up to an arbitrary channel count and number of egress ports: the structure enables non-blocking transparent wavelength-selective switching, with the capability of routing each individual channel of the input signal to an arbitrary port, without any routing conflict or blocking configuration.

The architecture is based on a divide and conquer approach, separating the demultiplexing and switching operation into multiple symmetric and independent blocks, which allows design flexibility and tailoring to the required scenario. The main functional blocks are depicted in Fig. 1 for the S+C+L implementation scenario, and depict all the sub-circuits from the input port up to the egress port multiplexers. Moreover Fig. 2 the internal structures of the functional blocks, highlighting the cascading structure of the multiplexer filters, as well as the binary tree switching networks used for the routing operation.

This structure has been developed to minimize crosstalk and channel interference, as well as allow precise design and optimization of the sub-blocks for each band of interest: by dividing the switching operation and multiplexing into parallel structures, while the redundancy and element count increases, so too does the flexibility and tunability, allowing each sub-module to be designed for the required channel of interest.

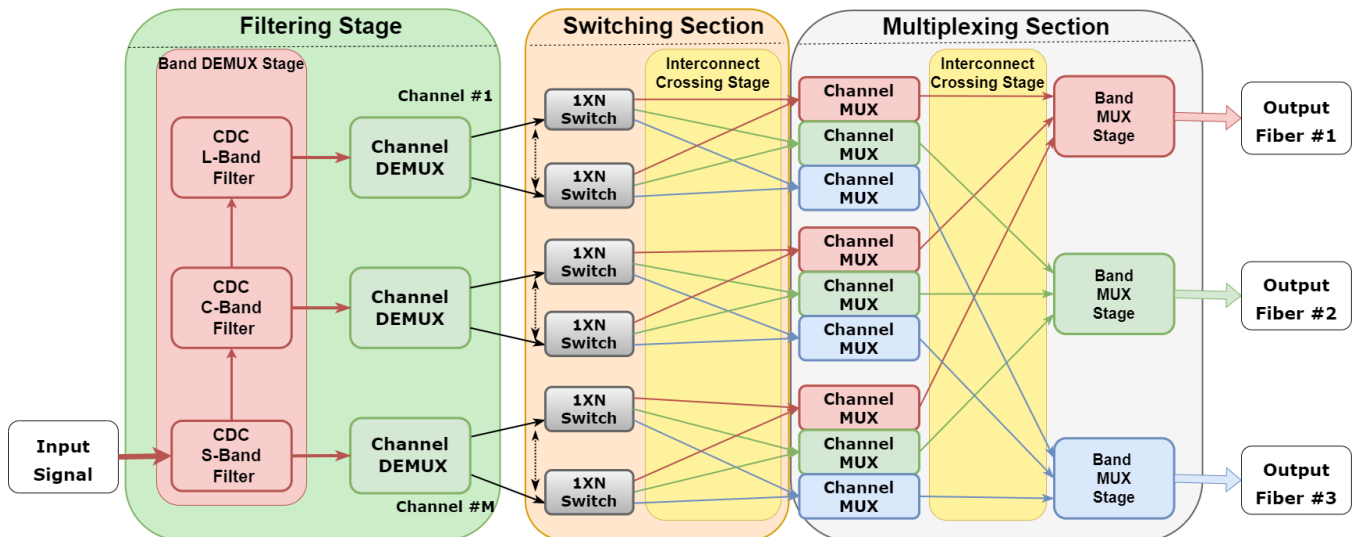Starting from the input signal, each band is filtered and routed

Fig. 1: Architecture of the 1×3 WSS.

to an independent channel demultiplexer, which is comprised of a cascade of individual channel filters, tasked with dividing each component of the WDM comb: the initial band division is done to reduce both the crosstalk, as well as the overall losses, allowing a shorter filter chain.

After the demultiplexing operation, each channel is routed by a 1×N binary-tree independent switching network, which send the signal towards the required output port: using parallel 1×N networks is more efficient with respect to large scale non-blocking topologies such as Beneš or Clos based switches, in particular for many input few output systems like WSS.

Following the switching operation each channel is multiplexed onto a common guide for each egress port, using a structure symmetric with respect to the input demultiplexer; moreover, the symmetric structure allows the losses to be balanced between the channels, as the optical path and number of traversed filtering element can be made equal for each channel of the comb.

The current architecture represents an improved and more robust version with respect to previous iterations [3], and it relies on two main building components, namely Grating Assisted Contra-Directional Couplers (GA-CDC) and Mach-Zehnder Interferometers (MZI). GA-CDCs are versatile structures [4] that can be used to implement flat-top non-periodic add-drop filters, which makes them ideal in DWDM applications, as they avoid many issues of traditional MicroRing-Resonator(MRR) based filters (side-channel aliasing, poor extinction ratio, high uncertainty sensibility). In this current iteration of the architecture, different CDCs are used for both the band division, as well as the individual channel Multiplexing/Demultiplexing [5].

The switching operation is instead carried through thermally-controlled MZI 1×2 switches, which represent a standard solution for wide-band frequency-independent applications

[6]: due to the previous demultiplexing stage, the switching stage is robust to fabrication uncertainty and can deploy relatively simple switching elements, as each channel is already filtered and separated from the comb, allowing a straightforward cross-bar routing system.

The only other elements in the architecture are the waveguide crossings between the output of the switching networks and the MUX stages, as highlighted in Fig. 1. These elements are modeled as lossy passive components, considering the state-of-the-art technologies in waveguide manufacturing [7].
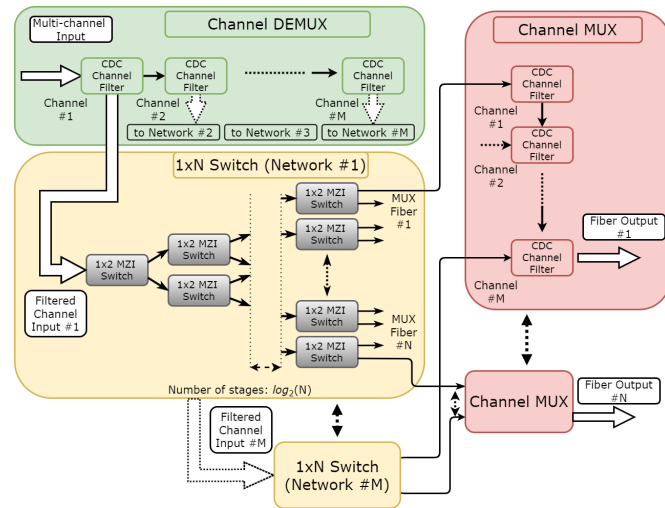

Fig. 2: Internal structure of the MUX/DEMUX and the switching architectures.

III. TRANSMISSION PENALTIES

Having defined the main architecture and components, we showcase the simulation results for a 24-channel implementation with 3 output ports.
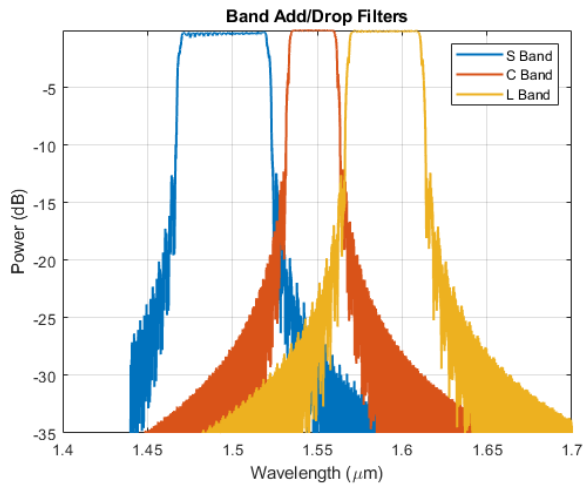
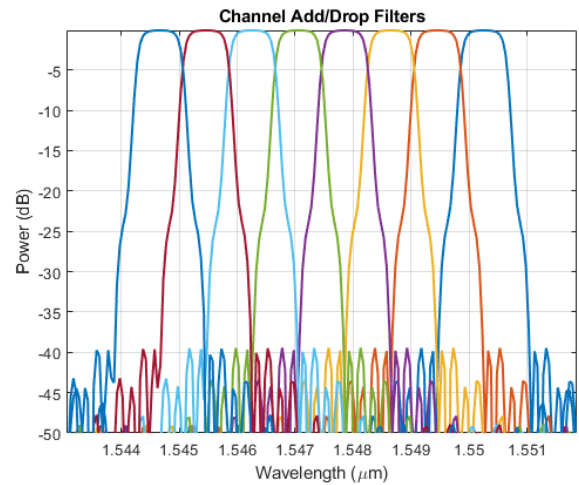Fig. 3: GA-CDC response for the three band MUX/DEMUX add-drop filters.

Fig. 4: Normalized GA-CDC response for the channel MUX/DEMUX add-drop filters.

The design of each component has been optimized for the reference channel, and each element has been simulated using multiple techniques, ranging from analytical models, CMT, BMP, and FDTD methods in order to properly verify the behavior and expected response. Simulations have been carried out using the RSoft$^{©}$ Photonic Simulation Suite [8], with the resulting data being used to create a circuit block model of the entire device. This circuit-level model has been run using the DSP-level simulation available in Optsim$^{©}$, allowing the characterization of the transmission impairments and losses. The simulations have been run considering the 400ZR standard, with Free-Spectral Range FSR=100 GHz, 16QAM modulation with symbol rate R_s=60 GBaud. The Bit-error Rate (BER) of the simulation was used to evaluate the Optica Signal-to-Noise Ratio degradation ΔOSNR with respect to the back-to-back system, considering a threshold BER$_{th}$=10^{-3}.

The penalty and transmission quality have been characterized considering two main components: the balanced component insertion loss, equal between all channels, and the path-dependant penalty, due to the channel filtering and waveguide crossings.

By the observing the response of the main band and channel filtering components (Fig. 3, Fig. 4), it's clear that the channel distortion is quite limited, due to the extremely flat-top and high extinction ratio profile of the CDC responses, and as such we expect a compatible behavior between the three bands of operation. The output spectrum of each channel, without considering the path-dependant waveguide crossing interconnects, is depicted in Fig. 5, and highlights the expected behavior due to the balanced MUX/DEMUX configuration present in the architecture. In previous network simulations of the architecture, using MRR-based elements [9] the insertion loss (IL) was instead different between channels, requiring a path-dependant model of the IL to properly characterize the transmission impairments.

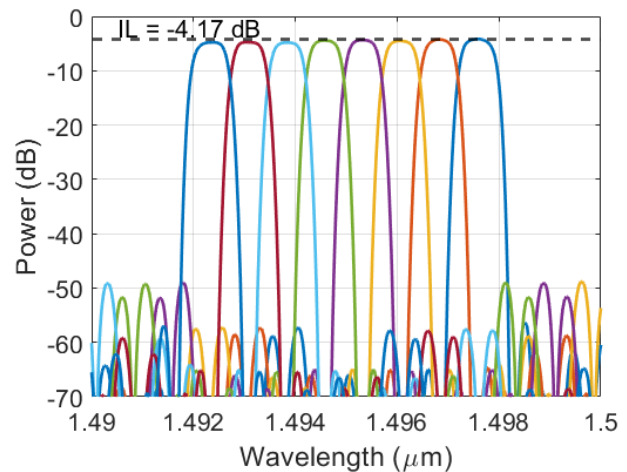In Fig. 6 the ΔOSNR penalties are depicted as a function of

Fig. 5: Output Frequency response and insertion loss (reference S-Band).

the number of encountered crossings, considering all possible routing configurations of each channel: as expected a linear dependency can be seen, due to the modeling of the waveguide interconnects as lossy elements. This highlights how penalties are mainly affected by the passive interconnects, whereas the channel shaping due to the filters and switches is almost constant for the different channels and bands. Moreover, in Fig. 7, an estimate of the circuit footprint is depicted considering the design size of the main components: the device is estimated to occupy a 2.1 mm×2.6 mm chip, considering standard tolerances and barrier between the different filtering and switching elements.

Overall, the device shows theoretical performances compatible with alternative WSS solutions described in the literature [10], but provides a more compact footprint and lower theoretical losses.
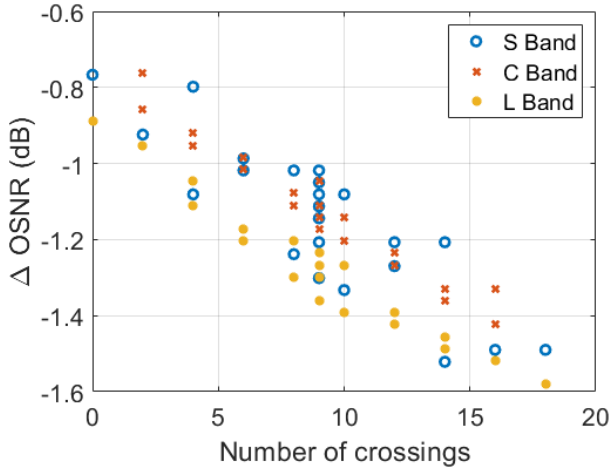
Fig. 6: OSNR penalty measured at the output for all possible routing configurations.
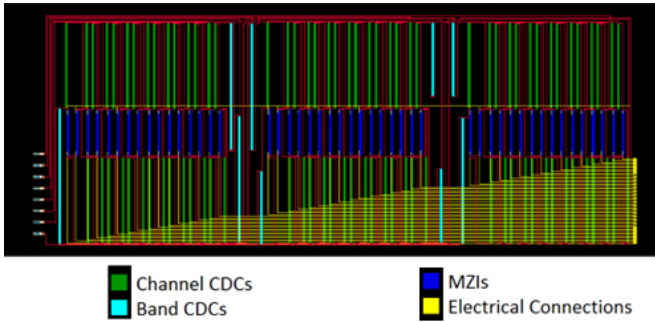

Channel CDCs   MZIs
Band CDCs   Electrical Connections

Fig. 7: Circuit footprint and mask for the 24 channel 3 port implementation (2.1×2.6 mm).

IV. CONCLUSIONS

We have proposed and demonstrated the operation and design principle for a PIC-based integrated WSS based on GA-CDC, allowing non-blocking independent routing of DWDM multi-band signals. The design and theoretical validation have been done using a variety of modeling techniques using standard approaches available in commercial-grade photonic simulation platforms. The resulting architecture has been simulated in a DSP-aware scenario to characterize its penalties and shows compatible results with the literature in terms of channel shaping while demonstrating a reduced footprint and lower insertion losses.

REFERENCES

[1] K. Kim, K.-H. Doo, H. H. Lee, S. Kim, H. Park, J.-Y. Oh, and H. S. Chung, "High speed and low latency passive optical network for 5g wireless systems," Journal of Lightwave Technology **37**, 2873–2882 (2018).

[2] A. Ferrari, A. Napoli, J. K. Fischer, N. Costa, A. D'Amico, J. Pedro, W. Forysiak, E. Pincemin, A. Lord, A. Stavdas *et al.*, "Assessment on the achievable throughput of multi-band itu-t g. 652. d fiber transmission systems," Journal of Lightwave Technology **38**, 4279–4291 (2020).

[3] L. Tunesi, I. Khan, M. U. Masood, E. Ghillino, A. Carena, P. Bardella, and V. Curri, "Novel design and operation of photonic- integrated wss for ultra-wideband applications," in *2022 IEEE Photonics Society Summer Topicals Meeting Series (SUM),* (2022), pp. 1–2.

[4] M. Hammood, A. Mistry, H. Yun, M. Ma, S. Lin, L. Chrostowski, and N. A. F. Jaeger, "Broadband, silicon photonic, optical add–drop filters with 3 dB bandwidths up to 11 THz," Opt. Lett. **46**, 2738–2741 (2021).

[5] H. Qiu, J. Jiang, P. Yu, D. Mu, J. Yang, X. Jiang, H. Yu, R. Cheng, and L. Chrostowski, "Narrow-band add-drop filter based on phase-modulated grating-assisted contra-directional couplers," J. Lightwave Technol. **36**, 3760–3764 (2018).

[6] I. Khan, L. Tunesi, M. U. Masood, E. Ghillino, P. Bardella, A. Carena, and V. Curri, "Optimized management of ultra-wideband photonics switching systems assisted by machine learning," Opt. Express **30**, 3989–4004 (2022).

[7] S. Wu, X. Mu, L. Cheng, S. Mao, and H. Fu, "State-of-the-art and perspectives on silicon waveguide crossings: A review," Micromachines **11** (2020).

[8] https://www.synopsys.com/photonic-solutions.html.

[9] L. Tunesi, I. Khan, M. U. Masood, E. Ghillino, A. Carena, V. Curri, and P. Bardella, "Photonic-integrated wavelength selective switch for S+C+L applications," in *Optical Components and Materials XX,* , vol. 12417 S. Jiang and M. J. F. Digonnet, eds., International Society for Optics and Photonics (SPIE, 2023), p. 124170X.

[10] R. Kraemer, F. Nakamura, M. v. d. Hout, S. van der Heide, C. Okonkwo, H. Tsuda, A. Napoli, and N. Calabretta, "Multi-band photonic integrated wavelength selective switch," J. Lightwave Technol. **39**, 6023–6032 (2021).